Modeling Airflow and Lift to Design a Wing for Human-Powered Flight

Alan Bruner, Evan Cochrane, Theodore Guetig, Ben Wilfong

Introduction

Using computers in the digital age for modeling and design work is vital to conserve time and resources. Modeling software's aerospace applications include evaluating current digital designs and furthering their development before implementing a physical prototype. This process is known as digital engineering and is becoming common practice in industry, including the United States Air Force. In this paper we design a human-powered aircraft by computing the lift generated by its wings using the computational software MATLAB to better understand the push towards digital engineering. The panel method is used for this task due to its low computational cost, compared with, say, a computational fluid dynamics approach. Panel methods provide accurate calculations of lift, but are unable to provide drag estimates.

Model

The power generated by a human is limited, and for this reason, human-powered flight requires careful selection of an airfoil that offers high lift coefficients at low speeds. The DAE11 airfoil was selected because it meets these desired characteristics and was implemented on the Daedalus project, which holds the current record for longest human-powered flight [3]. The panel method is used to approximate the lift of the DAE11 airfoil. This model does not include complex geometry or changing structural characteristics.

Image Processing

The airfoil's data points need to be extracted and loaded into MATLAB before running the computational model. A Sobel edge filter is first applied to the image, which can determine the general shape of the wing. This edge detection can leave gaps, so the output of the Sobel filter is then fed through a dilation function to ensure the edge is a single continuous shape.

Next, we find the airfoil's perimeter, which is then converted to a list of points. The dilated edge is first passed through a fill function, filling all pixels on the interior of the edge. The filled image is passed to MATLAB's **bwperim** function, which returns an image with filled pixels only along the perimeter
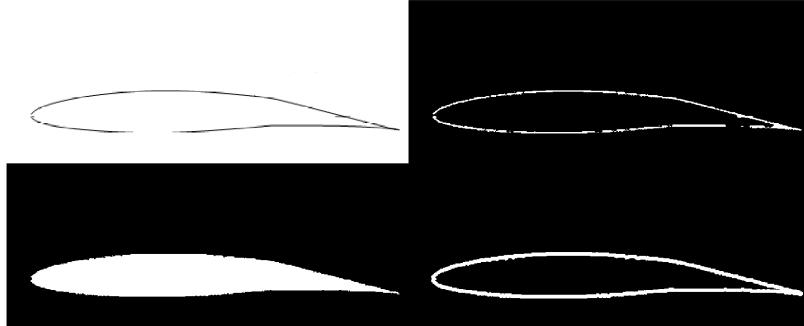
Figure 1: The steps taken to process an image. White pixels in the latter 3 images are filled pixels. **Top Left:** The original image **Top Right:** The results from the edge filter **Bottom Left:** The filled edge filter **Bottom Right:** The perimeter of the object

of any shapes in the image. Without filling the image, **bwperim** would fill pixels on both the inner and outer sides of the dilated edge filter. See Figure 1 for a visualization of the dilation, fill, and perimeter functions. The function **bwtraceboundary** is then used on the identified perimeter and returns an in-order list of all points along the perimeter starting at the lower right corner. The wake model follows from these points that describe the perimeter.

After pre-processing, the endpoints of the panels are found by tracing this perimeter. When a new point is placed, the function moves a number of pixels along the perimeter and calculates the angle between those two points. The function then continues along the perimeter, calculating the angle between the current location and the previously placed point at each step. If the current calculated angle is outside of a specific tolerance, then a new data point is placed at the current location, and a new comparison angle is calculated. This process continues until the entire perimeter has been traced. This method ensures that more points are placed along areas of the wing with greater curvature, which provides the most information when running the mathematical model on discretized profile.

In order to allow the user to select how many points the approximation should have, the function dynamically finds an angle tolerance which results in the desired number of points. This tolerance is found using a modified binary search algorithm. If the angle tolerance is too low, then the program generates more points than desired, while the reverse happens if the angle tolerance is to high. If too many points are found, then the angle tolerance doubles. If too few points are found, the angle tolerance is halved. This process repeats until the desired number of points are found. Figure 2 shows the resulting points of
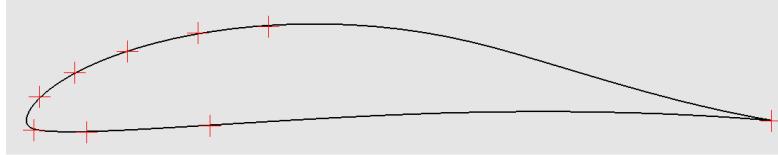
Figure 2: The resulting points of the point finding algorithm, shown as red crosses. The rightmost point is the tail.

a sample wing overlaid onto the original image.

Once the desired number of points are found, the program adds two more points: a repeat of the first (tail) point, and a point behind the tail to represent the end of the wake trail. The location of the wake trail point is calculated using a specified distance from the wake trail to the tail point and specified angle to the horizontal axis. This allows us to customize the wake trail, depending on the orientation of the wing.

Mathematical Model

We use the symbol Φ to denote the airflow at a given point in two-dimensional space with coordinates x and z, so the gradient $\nabla\Phi$ represents the velocity of the fluid at a given point. Over a region R, the rate at which the mass of fluid changes with time can be computed using the formula

$$\frac{dm}{dt} = \frac{\partial}{\partial t} \int_R \rho \, dV - \int_{bd(R)} \rho \nabla\Phi \cdot \mathbf{n} \, dS, \tag{1}$$

where $bd(R)$ is the boundary region of R, $\mathbf{n}$ is an outward facing normal vector, and ρ is the density of the air [1].

A number of simplifying assumptions are made to allow us to derive a formula for $\nabla\Phi$. We assume air is incompressible and homogeneous, i.e., constant density, so ρ is constant everywhere, and

$$\int_R \rho \, dV = 0.$$

We also know that the mass of the region does not change, $\frac{dm}{dt} = 0$, reducing (1) to

$$\int_{bd(R)} \nabla\Phi \cdot \mathbf{n} \, dS = 0.$$

By the divergence theorem, then,

$$\int_{bd(R)} \nabla\Phi \cdot \mathbf{n} \, dS = \int_R \nabla^2\Phi \, dV = 0. \tag{2}$$

3

The second integrand in (2) must be 0 if the integral is 0, which gives Laplace's equation for incompressible flow,

$$\frac{\partial^2 \Phi}{\partial x^2} + \frac{\partial^2 \Phi}{\partial z^2} = 0.$$

The only solutions to Laplace's equation are sources, sinks, and doublets. The streamlines for these solutions look like:
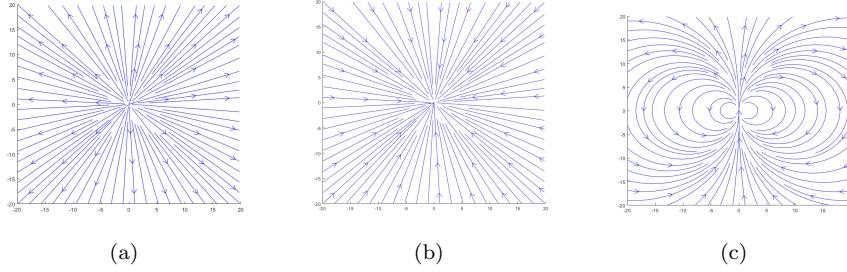

(a) (b) (c)

Figure 3: Source (a), sink (b), and doublet (c) solutions to Laplace's equation.

We only consider the doublet solutions Φ_d close to the wing and assume a known constant free stream velocity Φ_f far from the wing. The doublets are oriented so that a flat wing surface would be horizontal in the center of the picture in Figure 3(c). Our streamline calculation is then

$$\Phi \approx \int_C \mu \Phi_d \, dl + \Phi_f,$$

where C is a curve defining the two-dimensional wing cross-section and μ is the doublet strength. We approximate the streamline by replacing C with N linear panels, including a wake panel at the tail of the wing. This gives

$$\Phi \approx \sum_{j=1}^{N} \int_{L_j} \mu_j \Phi_d \, dl + \Phi_f, \tag{3}$$

where each L_j is a panel.

We assume the boundary condition

$$\mathbf{n} \cdot \nabla \Phi = 0, \tag{4}$$

which roughly corresponds to the velocity vectors being tangent to the wing, to solve for each doublet strength, assuming a constant doublet strength for each panel μ_j. Substituting (3) into (4) for each panel i gives

$$\sum_{j=1}^{N} \mu_j (\mathbf{n}_i \cdot \int_{L_j} \nabla \Phi_d \, dl) + \mathbf{n}_i \cdot \nabla \Phi_f = 0.$$

We then formulate this as a system of linear equations,

$$A\boldsymbol{\mu} = \mathbf{b},$$

where $\boldsymbol{\mu}$ is the vector of doublet strength to solve for, the matrix coefficients are

$$A_{ij} = \mathbf{n}_i \int_{L_j} \nabla\Phi_d \, dl$$

and the right-hand side is

$$\mathbf{b}_i = -\mathbf{n}_i \cdot \nabla\Phi_f.$$

All that is left to do is solve for each integral in the matrix A, and then solve the system. We make use of a collection point for panel j, say (x, z). An exact solution to each integral can be found by rotating and translating the wing for each L_i so that panel L_i is centered on the x axis with normal vector pointing in the $-z$ direction. We let d_i denote half of the length of panel i. Using the midpoint of each panel as the collection points, when $i \neq j$, the integral is

$$\int_{L_j} \nabla\Phi_d \, dl = \frac{1}{2\pi} \begin{bmatrix} \frac{z}{(x+d_j)^2+z^2} - \frac{z}{(x-d_j)^2+z^2} \\ \frac{x-d}{(x+d_j)^2+z^2} - \frac{x+d_j}{(x+d_j)^2+z^2} \end{bmatrix}$$

Using a collection point other than the midpoint gives a significantly longer formula, which we omit for brevity. Otherwise, when $i = j$,

$$\int_{L_i} \nabla\Phi_d \, dl = \frac{1}{2\pi} \int_{-d}^{d} \begin{bmatrix} 0 \\ \frac{-1}{a^2} \end{bmatrix} da.$$

Unfortunately, evaluating the second coordinate involves integrating over a singularity, and the resulting limit diverges. This is resolved by moving the translated collection point off the z-axis so the collection point for panel i is no longer on its own panel. Evaluating the integral with the new collection point gives

$$\int_{L_i} \nabla\Phi_d \, dl = \begin{bmatrix} 0 \\ \frac{-1}{\pi d_i} \end{bmatrix}.$$

Of course, these vectors need to be rotated and translated back to their original positions before taking their dot product with $\mathbf{n}$.

We approximate the circulation arround the wing Γ as the negative of the doublet strength of the wake panel, i.e., $\Gamma = -\mu_N$. By the Kutta-Joukowski Theorem, we can estimate the lift generated per meter of wing with a given cross-section as

$$F_l = \Gamma v \rho,$$

where v is the magnitude of the free stream vector and ρ is the density of the air. If the weight per meter of the wing is w_{wing}, and the weight of the fuselage is

w_f, we finally estimate how long our wing needs to be to counteract the weight of the plane by solving

$$Lw_{wing} + w_f = LF_l$$

for L.
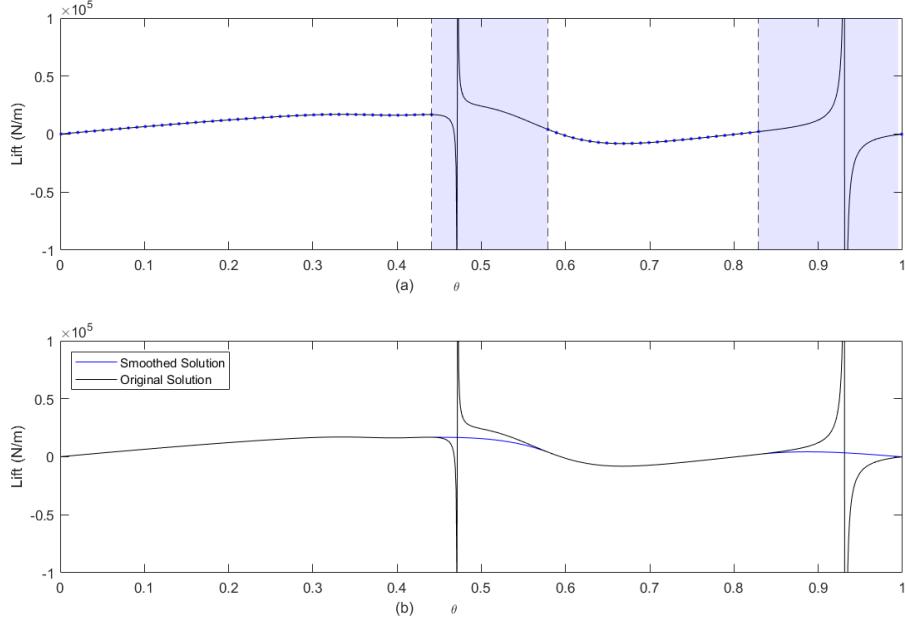
Results

Example Airfoil

Figure 4: Representative Sample of Spline Points

Initial results of lift as a function of the wing collection point for the panels in the second example in Chapter 8.3 of [1] included singularities due to numerical instabilities in the model. The horizontal axis in Figure 4 plots a parameter $\theta \in [0, 1]$ that uniquely determines the location of each collection point on the panel. If $\mathbf{x}$ is the endpoint closer to the front of the wing and $\mathbf{y}$ is the endpoint closer to the back of the wing for any panel, the collection point for that panel is a convex combination of $\mathbf{x}$ and $\mathbf{y}$,

$$\theta\mathbf{y} + (1 - \theta)\mathbf{x}.$$

We also use the parameter $\rho \in [0, 1]$ in the same way for collection point of the wake panel, which is treated seperately from the other panels. A cubic spline
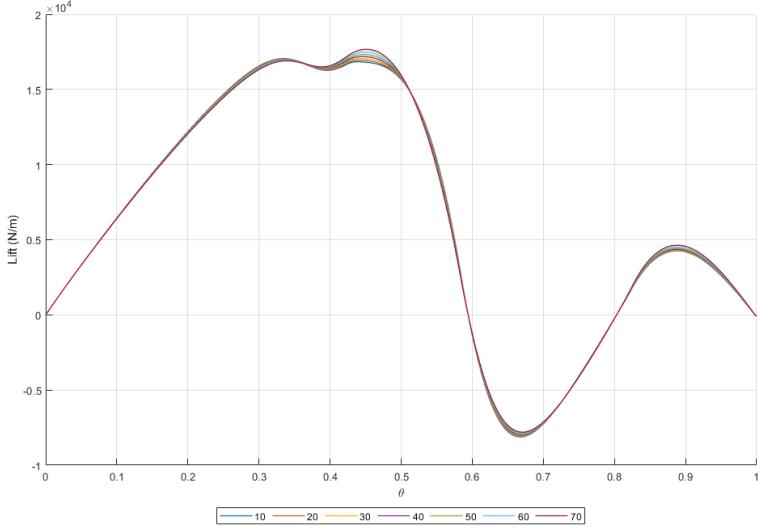
Figure 5: Lift Versus θ for a Range of Wake Angles

through one-tenth of the points in the regions of relatively slow change smooths these singularities. Figure 4 shows the results of this smoothing for the second example from the text with a wake angle of ten degrees. Figure 4a shows the spline points as blue dots along the original curve. The omitted regions are those shaded in light blue. The resulting cubic spline is graphed along with the original curve in Figure 4b. These singularities were also observed in the DAE11 airfoil computations.

We vary the wake's length, angle, and collection point to study the effects of the wake mode. Results from this search inform an initial guess for a constrained optimization problem then helps us to maximize lift. For each trial, lift is calculated as a function of θ on the main body of the wing with the intent to find a wake model and collection point that maximizes lift.

The first experiment explored the effect of wake angle on lift. The model was solved for wake angles ranging from ten to seventy degrees below horizontal in ten degree increments while the wake length and ρ were held constant at 0.957 m and 0.5, respectively. Results of this exploration are graphed in Figure 5. Table 1 summarizes the maximum lift values for each wake angle and the corresponding θ value.

Adjusting the wake angle had a relatively small effect on overall lift yielding a range of maximum lifts of only 340 N/m. The trend in maximum lift as a function of wake angle indicates a monotonically increasing lift trend for angles greater than 30 degrees. Examining the wing panel collection points also indicates that at low wake angles, the maximum lift occurs when collection points

7

Table 1: Wake Angle Summary

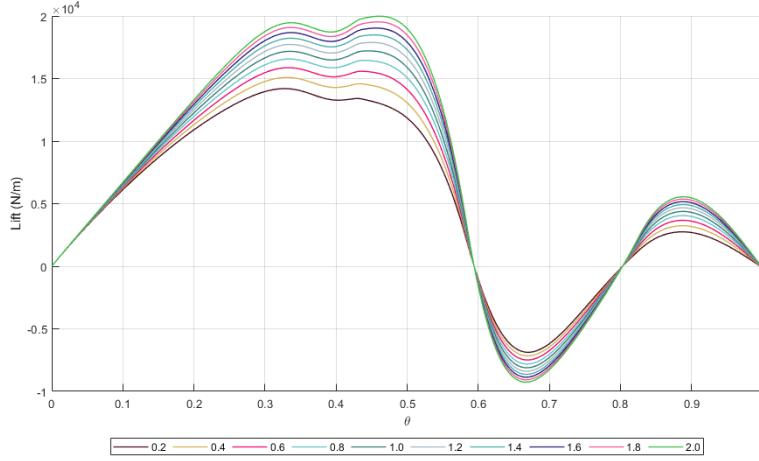| Wake Angle	10	20	30	40	50	60	70
Lift (kN/m)	17.05	17.06	16.99	17.01	17.06	17.18	17.33
θ	0.334	0.335	0.444	0.447	0.449	0.450	0.451

Figure 6: Lift Versus θ for a Range of Wake Lengths

closer to the front of the wing panels are used. For wake angles of 10 and 20 degrees below horizontal, the maximum lift occurs at the first peak in Figure 5. Beginning with a wake angle of 30 degrees below horizontal, the wing panel collection point corresponding to the maximum lift moves farther back on the panels, corresponding to the second peak in Figure 5.

The second experiment explored the effect of wake length on lift. The model was solved with wake lengths ranging from 0.2 to 2.0 meters in 20 cm increments while wake angle and ρ were held constant at 30 degrees and 0.5 respectively. Results of this exploration are graphed in Figure 6. Table 2 summarizes the maximum lift values for each wake length and the corresponding θ.

Adjusting the wake length had a larger effect on lift values than wake angle, yielding a range in maximum lift values of 3.11 kN/m. Plotting the maximum lift as a function of wake length gives the relationship shown in Figure 7. A local maximum in lift of 17.54 kN/m is achieved at 1.3 meters. The maximum lift remains relatively constant between 1.3 and 1.6 meters before beginning to decrease.

The third experiment explored the effect of changing the wake panel collection point on lift. We solved the model for ρ values ranging from 0.5 to 0.9 in increments of 0.1 while wake angle and length were held constant at 30 degrees and 0.957 m respectively. The graphical results of this exploration are provided

Table 2: Wake Length Summary

Wake Length	0.2	0.4	0.6	0.8	1.0	1.2
Lift (kN/m)	14.20	15.09	15.87	16.56	17.08	17.47
θ	0.328	0.331	0.333	0.334	0.446	0.450

Wake Length	1.4	1.6	1.8	2.0
Lift (kN/m)	17.50	17.52	16.81	15.90
θ	0.454	0.456	0.459	0.461
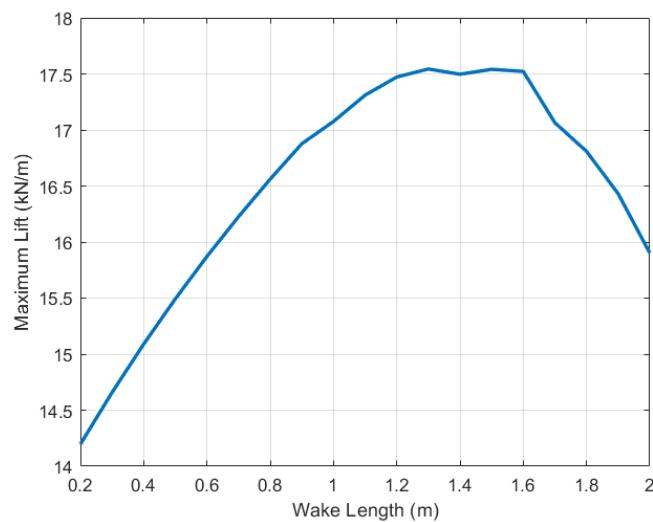
Figure 7: Maximum Lift vs. Wake Length
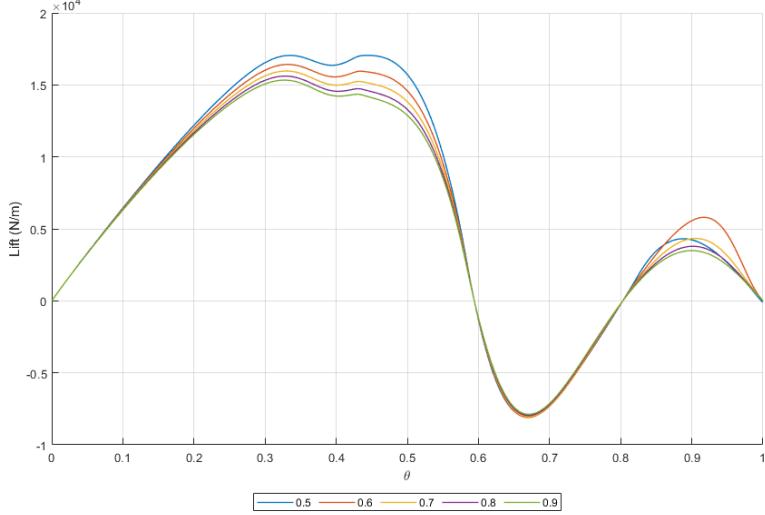
Figure 8: Lift versus θ for a Range of ρ

Table 3: Wake Collection Point Summary

ρ	0.5	0.6	0.7	0.8	0.9
Lift (kN/m)	16.99	16.42	15.96	15.61	15.33
θ	0.444	0.332	0.330	0.328	0.327

in Figure 8. Table 3 summarizes the maximum lift values for each wake length and the corresponding collection point on the wing panels.

The wake panel collection point had a relatively large effect yielding a range of maximum lift values of 1.66 kN/m. As the wake panel collection point moves towards the back of the panel, the optimal wing panel collection point moves closer to the front of the panel. Lift as a function of wing panel collection point was unstable for θ values of less than 0.5, so those values were omitted. In this range, maximum lift monotonically decreases with wake panel collection point.

Table 4 summarizes the maximum lift values from each of the three experiments. Wake length has the greatest effect on maximum lift, followed by wake

Table 4: Summary of Parameter Results

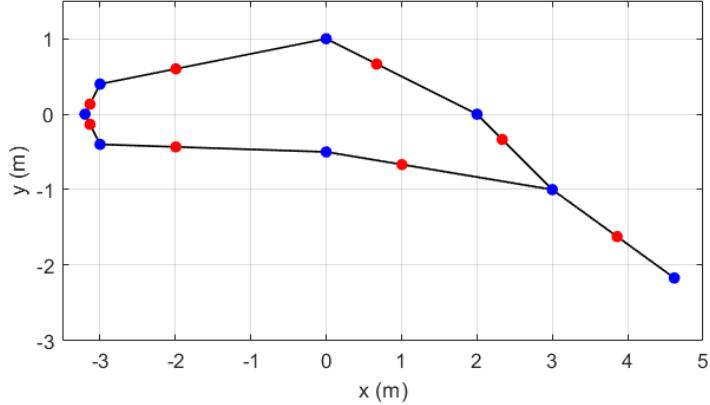| Parameter	Max (kN/m)
Angle	17.3
Length	17.3
Collection Point	17.0

Figure 9: Optimized panel model. Blue points are the endpoints of the panels, and red points are the collection points.

panel collection point and wake angle. The results of these three experiments suggests a wake model that produces maximum lift without distorting the wing should occur when the wake angle is near 30 degrees below the horizontal, the wake length is near 1.3 m, and the wake panel collection point is near 0.5.

The results of our experiments are used to define a constrained optimization problem to determine what parameter values would yield maximum lift. The following constraints were applied to the parameters:

$$0 \text{ degrees} \leq \text{Wake Angle} \leq 45 \text{ degrees},$$

$$0.2 \text{ m} \leq \text{Wake Length} \leq 2 \text{ m, and}$$

$$0.5 \leq \text{Wake Collection Point} \leq 0.9.$$

The resulting maximum lift of 18.77 kN/m occurred with the wake angle being 35.9 degrees below horizontal, the wake length being 1.997 meters, and ρ being 0.5313. The θ for this lift value was 0.335. The discretized cross-section is shown in Figure 9.

DAE11 Airfoil

To aid the design of a human powered aircraft, we use a 10 panel model of the DAE11 airfoil described previously with a chord length of 2.5 meters, wake
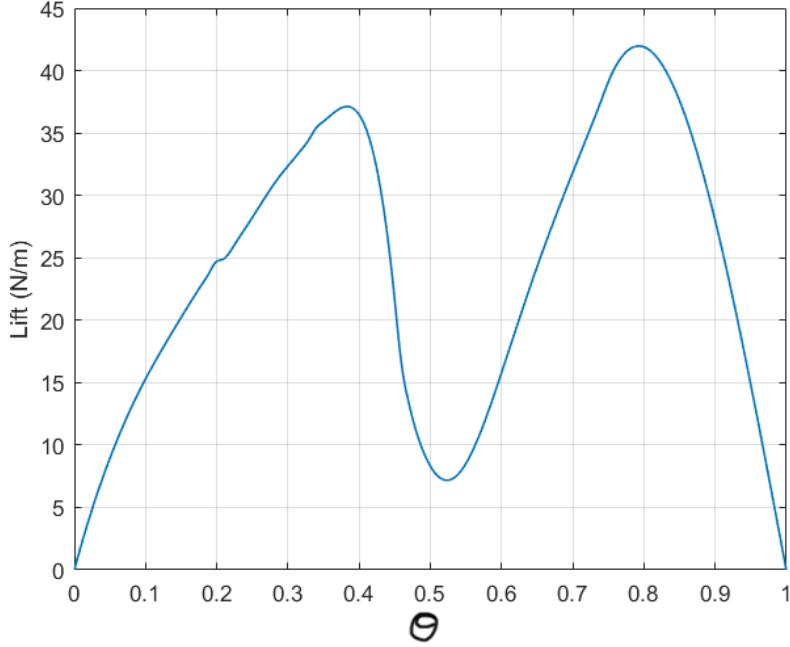
11

Figure 10: Lift Versus θ

angle of 35.9 degrees below horizontal, a wake length of 0.83 meters, a ρ value of 0.5313, an angle of attack of 5 degrees, and a free stream velocity of 6.7 m/s. The results of lift as a function of θ are in Figure 10.

There are two local maximimums in lift. The first is at a wing panel collection point of 0.384 yielding a lift of 37.11 N/m. The second is at a wing panel collection point of 0.794 yielding a lift of 41.97 N/m. At a wing panel collection point of 0.75, commonly used for these problems, the lift is 38.97 N/m. The maximum wing length can then be calculated given the fuselage mass, the passenger mass, and mass per unit length of the wing structure. The required length is given by the following equation:

$$L = \frac{w_f + w_p}{F_l - w_{wing}},$$

where L is the length of the wing, w_f is the fuselage weight, w_p is the passenger weight, F_l is the lift force per unit length produced by the wing, and w_{wing} is the weight per unit length of the wing. For a fuselage weight of 32 lbs (142 N), a passenger weight of 160 lbs (711 N), and a wing mass per unit length of 5.2 N/m inspired by the Daedalus project [2], this equation becomes

$$L = \frac{853}{F_l - 5.2}.$$

12

Table 5: Wing Length at Specific Collection Points

θ	F_l (N/m)	L (m)
0.384	37.11	26.73
0.750	38.97	25.26
0.794	41.97	23.20

The required wing length for each collection point is tabulated in Table 5.

The peak in lift that occurs at a wing panel at $\theta = 0.794$ is very sensitive to the region omitted from the cubic spline. The previous experiments suggest that maximum lift occurs when the wing panel collection point is near 0.34, so we assume the wing length of 26.73 meters associated with the $\theta = 0.384$ is the correct estimate.

Conclusion

Our results suggest that the panel method is an adequate model for calculating lift, especially for the computational resources needed for the estimations. It does not, however, provide any information on drag. We calculated a uniform cross-section wing length of 26.73 meters for a DAE11 airfoil at an angle of attack of 5 degrees and a free-stream velocity of 6.7 m/s. In the Daedalus project, a successful human powered craft was created with a wing span of 34.14 meters [2]. The panel method predictions are of the same order of magnitude as this successful example, suggesting the result is reasonable. A major advantage of the panel method is its computational speed. Past experience suggests that two-dimensional computational fluid dynamics models can take seconds to minutes to run while the panel method approach takes only fractions of a second. The advantage becomes even greater in higher dimensions.

Summary

In our paper, we use computational methods to estimate the length of a wing needed on an aircraft to achieve human-powered flight. The core model takes a two-dimensional cross-section, or airfoil, of the wing and computes the approximate lift generated per meter of wing. The outline of the airfoil is approximated as a series of discrete linear panels, including a fictitious wake panel at the back of the wing. Airflow is modeled as a doublet solution to Laplace's equation near the wing and wake, and a constant free stream velocity far from the wing. The doublet strengths for each panel are then computed by solving a system of equations whose coefficients are determined by integrating the airflow over each panel with respect to a collection point located somewhere on that panel. The doublet strength of the wake panel is the negative airflow around the entire wing, and lift can be calculated from airflow using the Kutta-Joukowski Theorem.

We use a picture of the DAE11 airfoil, a cross-section of the wing used on the Daedalus project, which holds the world record for the longest human-powered flight. We use image processing techniques to convert the airfoil image into a sequence of 11 points that represent the endpoints of the panels that approximate the airfoil's outline. The magnitude and velocity of the free stream vector, equivalent to the speed of the plane and angle of attack, the weight of the fuselage, weight of the pilot, and the weight of the wing per meter are fixed parameters that we choose to model the actual Daedalus project. These values are 6.7 m/s, 5 degrees below the horizon, 142 N, 711 N, and 5.2 N/m, respectively. The length and angle of the wake panel, the location of the collection point for each non-wake panel, and the location of the wake collection point are all parameters to the model that we search over to find an optimal lift.

Certain values of the parameter θ that we use to determine the collection point of each non-wake panel in particular cause singularities, so every computation is calculated over a range of θ values and the singularities are removed by replacing the resulting graph of lift v. θ with a cubic spline. Using a test airfoil, the optimal wake length is 1.997 meters, the optimal wake angle is 35.9 degrees below the horizon, and the optimal wake collection parameter is $\rho = 0.531$. This optimum occurs at $\theta = 0.384$. Running our model on the DAE11 airfoil with the above parameters gives a lift of 37.11 N/m, resulting in an estimated 26.7 meter wing required for takeoff. This is a decently close approximation of the 34 meter wing used in the actual Daedalus project, especially after considering that this model does not account for drag.

References

[1] Allen Holder and Joseph Eichholz. *An Introduction To Computer Science*. International Series in Operations Research & Management Science. Cham, Switzerland: Springer, 2019.

[2] John McIntyre and Pat Lloyd. *Man's Greatest Flight*. URL: `https://web.mit.edu/drela/Public/web/hpa/SG_HPAG_daedalus.pdf`. (accessed: 03.11.2022).

[3] Airfoil Tools. *DAE-11 Airfoil (dae11-il)*. URL: `http://airfoiltools.com/airfoil/details?airfoil=dae11-il`. (accessed: 03.12.2022).